Impact of coherence in radiation from ultrahigh-field atomic ionization

Isaac Ghebregziabher and Barry C. Walker
Department of Physics and Astronomy, University of Delaware, Newark, Delaware 19716, USA
(Received 16 October 2007; published 26 February 2008)

We quantify interference effects on radiation by calculating the angle- and energy-resolved Larmor radiation from atomic ionization in the focus of ultraintense field. Our calculations use a Monte Carlo classical and semiclassical tunneling probability current models of ionization for intensities in the range of 10^{16} to 10^{20} W/cm^2. For nonrelativistic intensities, whether the radiation from the photoionization is treated coherently or incoherently, classically or semiclassically, leads to a negligible effect on radiation. For relativistic intensities, coherently summing across the tunneling ionization probability current decreases the radiation by an order of magnitude when compared to classical ionization or incoherent summation of the radiation from the tunneling ionization probability current. The interference effect is most pronounced for high-energy photons since ionization and the electron quiver may be 1 μm and extends over multiple radiation wavelengths.

DOI: 10.1103/PhysRevA.77.023417 PACS number(s): 32.80.Rm, 42.65.Ky

I. INTRODUCTION

With the advent of tabletop ultrafast laser systems capable of delivering intensities exceeding 10^{19} W/cm^2 [1–6], we have began to witness observation of unique physical phenomenon in the ultrahigh intensity regime. Current experiments include the creating of multi-MeV heavy ions and protons [7], photonuclear fission [8], extreme ionization of atomic clusters [9], relativistic laser-plasma interactions [10], and new applications to plasma waveguides [11]. The future directions [12] of ultraintense laser science have broad frontiers that stretch to include fusion energy development and astrophysics. Some of the most fundamental ultraintense field physics involves the interaction of the ultrastrong field with the atom. This interaction, for example, addresses the scattering of relativistic electrons [13,14] by a high intensity laser produced via ionization in its focal region [15–17]. In this interaction photoelectrons ionized in an ultrastrong field ($>10^{18}$ W/cm^2) [18–20] quiver with a velocity close to the speed of light, the magnetic field of the ionizing laser field becomes significant and the motion of these ionized free electrons is nonlinear. It has been proposed to use the nonlinear motion of relativistic electrons inside the laser field to produce high-order harmonics of the incoming laser light [21] and there is a growing interest in the physics of the radiation from laser acceleration of photoionization [22–26] at "relativistic intensities." Recent theoretical work [27], based on Dirac charge current and classical electrodynamics, studies scattered radiation from a laser driven arbitrarily prepared Dirac wave packet and has shown deviations to purely classical calculations in the high-frequency part of the scattered spectrum.

The purpose of the paper is to clarify the impact of an incoherent versus a coherent treatment of the radiation from photoelectrons when the ionization, i.e., tunneling, is coherently driven. Though there are some indications from plasma experiments the process may be incoherent [28], it is not known experimentally whether radiation from coherently ionized and field accelerated photoelectrons in ultrastrong fields is incoherent, coherent, or partially coherent. This paper reports a theoretical investigation contrasting a classical treatment of the atomic process with semiclassical, incoherent, and coherent treatments. We employ the semiclassical trajectory ensemble model to represent the electron wave function in the continuum, which has been successful in predicting correlated multielectron ionization [29] and the cutoff photon energy associated with higher-order harmonic generation [30]. The results are presented here for 800 nm laser radiation, but similar results are expected for other visible and IR laser wavelengths [31,32].

The results presented extend previous works of an electron interacting with an intense electromagnetic field [33–40] by including the ionization process itself. We compare the traditional classical treatment of the electron in the continuum with that of a semiclassical current distribution treatment that includes interferences of the extended electron wave function in the continuum. We also address how the coherence can significantly change the spectral power and angular distribution expected from atoms in ultrahigh fields. Since the photoelectron dimensions are on the length scale of the driving-field wavelength, interference when emitting light could lead to enhancement and/or reduction of the emitted light depending on the coherence.

II. METHODOLOGY

The ultrastrong radiation model we use here is divided as follows: atomic photoionization, electron dynamics for the photoelectron in the continuum, and calculation of the radiation from the accelerated relativistic motion of the photoelectrons across the laser field. The laser pulse used for these calculations ($\mathbf{E}_{\text{laser}}$, $\mathbf{B}_{\text{laser}}$, linear polarization, 800 nm central wavelength, and 20 fs full width at half maximum Gaussian temporal profile) is comparable to current high-field experiments [41,42]. The two different spatial modes considered are a plane wave and $f/1.5$ TEM_{00} nonparaxial laser focus calculated to a field accuracy of 0.5%, i.e., third order nonparaxial terms [43,44]. Two models of ionization are considered: a classical model based on Monte Carlo tunneling and a semiclassical model using a trajectory ensemble adaptation of tunneling. The ionization contribution is generally considered from a single charge state; Ne^{8+} at 2×10^{17} W/cm^2,

Ar^{10+} at 2×10^{18} W/cm^2, Ar^{16+} at 1.2×10^{19} W/cm^2, Na^{10+} at 5×10^{19} W/cm^2, and Na^{11+} at 1.2×10^{20} W/cm^2. Results for ionization from multiple charge states preceding the peak intensity have also been calculated [45] but do not differ significantly from a single charge state result. These ions were chosen because they have a net ionization probability at the specified intensity of typically 10^{-3} to 10^{-2}. A cluster of 32 Opterons with 2.4 GHz processors were used for these calculations.

Radiation from the photoionization of a single atom is calculated with classical (*C*) and semiclassical (SC) treatments. For the semiclassical case, the radiation from the extended ionization current of the photoelectron is summed two ways, "incoherently" and "coherently," to contrast the differences between these two interpretations of how the photoelectron may radiate. We then proceed to calculate the emitted radiation from atoms in a realistic three-dimensional (3D) laser focus. The focal geometry calculations from many atoms are directly comparable to the results expected from experiments.

A. Classical and semiclassical ionization dynamics

For classical calculations, we merge strong field tunneling ionization with a Monte Carlo (MC) technique which has been described in [45]. Briefly, the tunneling ionization rate during the laser pulse is calculated according to the ionization based on hydrogen orbitals extended to complex atoms by Ammosov, Delone, and Krainov (ADK) [46]. The ADK theory is essentially an extension of Perelomov, Popov, and Terent'ev (PPT) [47] theory where states of complex atoms are characterized by effective principal and orbital quantum numbers. The tunneling ionization treatment used in this paper limits the maximum intensity to approximately 10^{20} W/cm^2, beyond this intensity the laser magnetic field and relativistic effects may affect the fundamental ionization mechanism [48]. No experimental measurements have verified the atomic ionization mechanism above a few times 10^{19} W/cm^2. Whether or not ionization occurs "at this phase" is determined by a weighted random number generator. When ionization occurs a single classical electron, i.e., a point charge, is liberated at the location of the atom from the bound state to the continuum. Over many ionization events, the MC ADK mechanism provides a linear mapping of the classical ionization to the ADK tunneling rate [45].

For semiclassical calculations, ionization for a single atom is calculated according to ADK tunneling for each phase of the laser pulse. Rather than a discrete ionization event as in the MC ADK case, here a trajectory ensemble weighted by the fractional ionization probability for that phase is liberated to the continuum. In this semiclassical ionization model, the trajectory ensemble weighted by the ionization probability is an approximation for the tunneling probability current of the quantum electron. In Fig. 1(a) the appearance of the electron probability in the continuum is plotted as a function of time and shown to be very similar for the classical MC ADK and semiclassical ADK calculation. It is important to note the MC ADK classical ionization case (which for a single event is a step function) is shown for

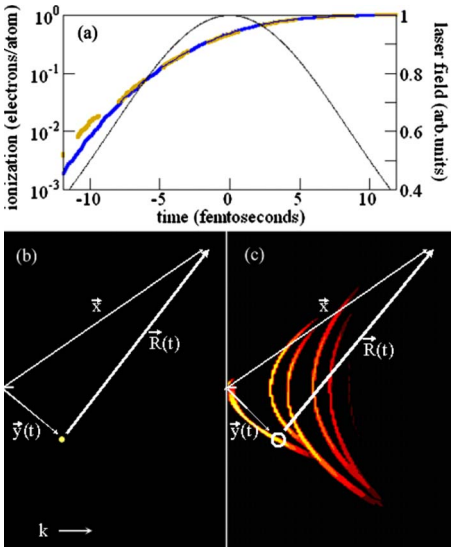

FIG. 1. (Color online) Plot of ionization probability (a) as a function of time across the laser pulse (thin line) for the MC tunneling (dashed) classical model and tunneling ionization probability current (wide line) semiclassical tunneling. Shown in (b),(c) are 2D plots of the electron density for a classical electron [dot, (b)] and the tunneling ionization probability current (c) in a 75 nm (horizontal, *k*) by 800 nm (vertical, *E*) frame from an atom ionizing (located at the white tick on the left center of each frame) a few cycles after ionization begins. Superimposed on the frames are the vector *x*, *y*, and *R* for the case when the atom is located at the origin. In (c) a representative charge segment $f_j q$ is circled in white.

many MC events and so represents an average. In Figs. 1(b) and 1(c) the spatial distribution of the electron probability after a single atom interacts with the field for few cycles is shown. While classical ionization gives rise to a single point electron [Fig. 1(b)] the tunneling ionization current appears continuously [Fig. 1(c)] with maximum bursts at the peaks of the electric field.

For both classical and semiclassical ionization methods, the photoelectron dynamics are calculated by solving the relativistic equations of motion in the laser electric and magnetic field. We use a Runge-Kutta ordinary differential equation solver with relative error tolerance threshold of 10^{-6}, local error threshold of 10^{-12}, and time step typically of the order 10^{-4} fs. Since the motion is on the scale of nm to μm and the electron energies are of order 10 times the ionization potential energy, the Coulomb field of the core atom or ion does not affect the dynamics. Also the interaction is considered in the low-density limit so space charge effects and hard collisions (collisions with low impact parameters) are neglected. Radiation damping is not accounted for in the calculation since the ratio of the total radiated energy per cycle to the average kinetic energy of the electron is less than 10^{-6}.

B. Superposition of the radiation

Classically the emitted electric field measured at an observers position $\vec{x}$ from a relativistically moving charge q with a trajectory $\vec{y}(t)$ is obtained from the Lienard-Wiechert potential [49] given by

$$\vec{E}(\vec{R},t) = \frac{q}{4\pi c}\left(\frac{\vec{n}\times[(\vec{n}-\vec{\beta})]\times\dot{\vec{\beta}}}{(1-\vec{n}\cdot\vec{\beta})^3|\vec{R}|}\right), \quad (1)$$

where $R(t)=|\vec{x}-\vec{y}(t)|$, $\hat{n}=[\vec{x}-\vec{y}(t)]/R(t)$, $\beta(t)=\dot{\vec{y}}(t)/c=(1/c)(dy/dt)(t)$, and c is the speed of light. Since $|\vec{x}|\gg|\vec{y}|$, $R^2\cong|\vec{x}|^2$. For the purposes of comparison, all reported fields and radiated energies are normalized for a yield expected from a single electron. The vectors $\vec{x}$, $\vec{y}(t)$, and $\vec{R}(t)$ are shown superimposed on Figs. 1(b) and 1(c).

In the plane wave (1D) classical ionization case the yield we report in this paper represents an average of hundreds to thousands of Monte Carlo photoelectrons for atomic ionization across a broad range of phases. Most of the radiation comes from electrons ionized at the peak of the field, however, the method accurately accounts for "off peak" ionization rates. For a single MC ADK ionization event, the emitted electric field is given by Eq. (1). For a number of atoms ionized N, the total radiated energy is the classical total radiated energy, W_C, per unit solid angle normalized to an average yield per photoelectron given by

$$\frac{dW_C}{d\Omega} = \left(\frac{c}{4\pi}\right)\frac{R^2}{N}\sum_{i=1}^{N}\int_{-\infty}^{\infty}|\vec{E}_i(\vec{R},t)|^2dt. \quad (2)$$

In the plane wave semiclassical treatment a single atom is adequate to accurately capture the emitted field response from the ionization current since ionization occurs over all phases; however, the normalization for the fractional ionization must be correctly taken into account. For a total number of M phase steps that comprise the semiclassical ensemble, the radiated electric field from the jth phase step of the ensemble $\vec{E}_j(\vec{R},t)$ is obtained by replacing q in Eq. (1) with the weighted charge $f_j\,q$, where f_j is the fractional ionization probability at a given laser phase [see Fig. 1(c)]. For incoherent and coherent superposition of the radiation from the tunneling probability current, the sum of the radiation and normalization must be done differently. For the incoherent case, the total radiated energy per unit solid angle from the SC tunneling probability ionization current is given by

$$\frac{dW_{\text{SC-incoherent}}}{d\Omega} = \left(\frac{c}{4\pi}\right)R^2\int_{-\infty}^{\infty}\left\{\frac{\sum_j^M(\vec{E}_j(\vec{R},t))^2}{\sum_j^M f_j^2(t)}\right\}dt. \quad (3)$$

In the case of a coherent superposition of the radiation from the tunneling probability current, $\vec{E}_j(\vec{R},t)$ must be summed before being squared to allow for interference, i.e., $\vec{E}_{\text{SC-coherent}}(\vec{R},t)=\Sigma_{j=1}^{M}\vec{E}_j(\vec{R},t)$. The total radiated power per single electron ionization event is then calculated by normalizing to the total ionization probability squared,

$$\frac{dW_{\text{SC-coherent}}}{d\Omega} = \left(\frac{c}{4\pi}\right)R^2\int_{-\infty}^{\infty}\left\{\frac{\left(\sum_j^M\vec{E}_j(\vec{R},t)\right)^2}{\left(\sum_j^M f_j(t)\right)^2}\right\}dt. \quad (4)$$

Here again M is the sum over the SC ensemble, not the sum over the ionization from different atoms.

The previous cases [Eqs. (1)–(4)] address the radiation from the interaction of the atom with a plane wave. Calculations for atoms distributed in a three-dimensional (3D) laser focus include an addition spatial sum for the radiation across all the ionizing atoms in the focus. Spatial summations for radiation between different atoms in all cases (i.e., W_C, $W_{\text{SC-incoherent}}$, $W_{\text{SC-coherent}}$) are done coherently; the total radiation field is equal to the sum of the fields from all the atoms. For the classical case, the form of Eq. (2) is the same, but the index N represents a sum of all ionization events across the focus and not an average of many atoms at a single location as for the plane wave case. In the SC tunneling probability current case, an additional sum is included over the N atoms ionizing in the laser focus incorporated as shown in Eqs. (5) and (6). It is important to note that $W_{\text{SC-incoherent}}$ in the focal geometry case involves an incoherent sum of the radiation from the tunneling ionization probability for a single atom but a coherent sum of the radiation between different atoms. For the fully coherent case $W_{\text{SC-coherent}}$, the radiation sums from the tunneling probability current and between atoms are treated coherently,

$$\frac{dW_{\text{SC-incoherent}}}{d\Omega} = \left(\frac{c}{4\pi}\right)R^2\int_{-\infty}^{\infty}\left\{\frac{\sum_i^{NM}\sum_j(\vec{E}_j(\vec{R},t))^2}{\sum_i^{NM}\sum_j f_j^2(t)}\right\}dt, \quad (5)$$

$$\frac{dW_{\text{SC-coherent}}}{d\Omega} = \left(\frac{c}{4\pi}\right)R^2\int_{-\infty}^{\infty}\left\{\frac{\left(\sum_i^{NM}\sum_j\vec{E}_j(\vec{R},t)\right)^2}{\sum_i^{N}\left(\sum_j^{M} f_j(t)\right)^2}\right\}dt. \quad (6)$$

With respect to scaling, without normalization the radiated power scales as N for the incoherent W_C and $W_{\text{SC-incoherent}}$ cases and as N^2 for the $W_{\text{SC-coherent}}$ case.

III. RESULTS AND DISCUSSION

A. Total radiated energy and power spectrum in a pulsed plane wave laser field

Figure 2 shows the total radiated energy from a photoelectron in a one-dimensional plane wave laser pulse with the three different treatments of the radiation: classical photoionization, and the tunneling probability current summed incoherently and coherently. The radiation yield in the figure is given in units of energy per photoelectron (eV/electron). The results are discussed in terms of three different intensity regimes [45] based on the relative size of the electron quiver motion ($\alpha_0=a_0\lambda/2\pi$, where $a_0=e\mathbf{E}_0/m\omega c$) to the wavelength of the emitted radiation $\alpha_0<\lambda/10$ region I, $\lambda/10<\alpha_0<\lambda$ region II, and $\lambda\leqslant\alpha_0$ region III.

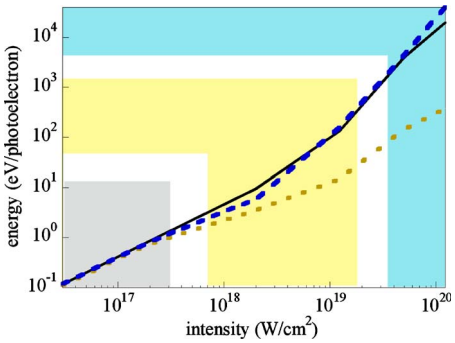

FIG. 2. (Color online) Radiated energy versus laser intensity from a classically ionized electron (solid, black), incoherently summed tunneling probability current (dashed, blue) and coherently summed tunneling probability current (dotted, dark yellow).

At intensities of 10^{17} W/cm^2 (α_0=38 nm) and less, highlighted as region I in the figure, the quiver amplitude is small. In this region, the total radiated energy from a photoelectron, whether classical, semiclassical, coherent, or incoherent, is identical. The quiver amplitude is sufficiently small that interference effects in the radiation are negligible. For laser intensities in the range (10^{17} W/cm^2 to 10^{19} W/cm^2, Fig. 2 region II) the electron quiver may be up to 300 nm. The total radiated energy from a classically ionized electron is still identical to the incoherently summed SC tunneling probability current. However, interference effects in the coherent sum reduce the radiated energy from one-half to one-fifth of the incoherent treatments.

Finally, for laser intensities greater than 10^{19} W/cm^2 (Fig. 2 region III), the electron quiver width exceeds the fundamental wavelength. Figure 2 shows for this intensity region the radiated energy from a classically ionized electron and incoherent sum of the tunneling probability current are indistinguishable. Continuing the trend from region II the coherently summed radiation from the tunneling probability current is 50 times smaller than incoherently summed radiation at an intensity of 1.2×10^{20} W/cm^2. This is attributed to the 1 micron electron quiver amplitude that results in significant interference effects.

Figure 3 shows the power spectrum of the radiated energy (Fig. 2) for intensities [Fig. 2(a)] 2×10^{17} W/cm^2, [Fig. 2(b)] 1.2×10^{19} W/cm^2, and [Fig. 2(c)] 5×10^{19} W/cm^2 with the three models of ionization MC ADK, SC incoherent, and SC coherent. From the figure, one can see the power spectrum calculated with classical MC ADK ionization and SC-incoherent model are identical. The radiated power drop at higher intensities seen in Fig. 2 for the coherent sum are manifested as a progressive decrease in the relative high-frequency radiation in Figs. 3(a)–3(c). While in Fig. 3(a) the power spectrum for all cases is nearly identical, in Figs. 3(b) and 3(c) the higher frequency radiation is lower by an order of magnitude. This observation corroborates the earlier interpretation of destructive interference for relativistic intensities where the photoelectron excursion is equal to or exceeds the wavelength of the radiation and results in a significant phase shift. The spectral amplitude from coherent averaging over the tunneling probability current is about a factor of 10 less

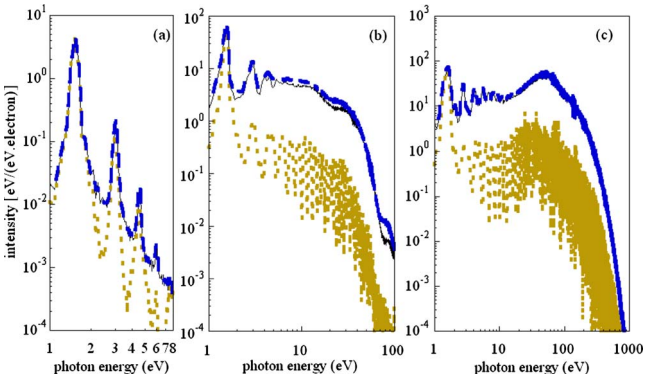

FIG. 3. (Color online) Total spectral amplitude of the radiated field from atomic ionization at intensities (a) 2×10^{17} W/cm^2, (b) 1.2×10^{19} W/cm^2, and (c) 5×10^{19} W/cm^2 from a classically ionized electron (solid, dark yellow), incoherently summed tunneling probability current (dashed, blue), and coherently summed tunneling probability current (dotted, black).

than that from a classically ionized electron. For higher energy photons with $\lambda<\alpha_0$, the spectral amplitude from a classically ionized electron is as large as 35 times that of a coherent average over an ionization probability current. In all cases, up to the maximum intensity of 10^{20} W/cm^2 studied, there is no observed difference in the integrated scattered fundamental radiation.

B. Angle resolved radiated energy from ionization in a pulsed plane wave laser field

The polar angle (θ measured from the k vector of the drive laser field) resolved total radiated energy is shown in Fig. 4 from a single classical electron and a tunneling probability current summed coherently in a one-dimensional plane wave laser pulse. (The incoherently summed ionization current result is indiscernible from the classical case.) The

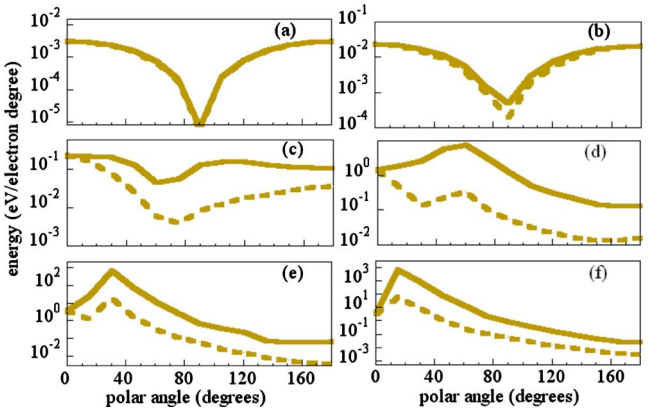

FIG. 4. (Color online) Angle-resolved radiated energy for ionizations in plane wave laser field with peak intensities (a) 3×10^{16} W/cm^2, (b) 2×10^{17} W/cm^2, (c) 2×10^{18} W/cm^2, (d) 1.2×10^{19} W/cm^2, (e) 5×10^{19} W/cm^2, and (f) 1.2×10^{20} W/cm^2 for a classical photoionization (solid) and coherently summed tunneling probability current (dotted).

radiation yield in the figure is given in units of energy per photoelectron per unit angle (eV/photoelectron degree). At laser intensities from 3×10^{16} W/cm^2 to 2×10^{17} W/cm^2 [Fig. 3(a) and 3(b)], the electron motion is nonrelativistic with $\gamma=(\sqrt{1-v^2/c^2})^{-1}\approx1.01$ to 1.05 and the interaction can be treated in the dipole limit, i.e., the radiated energy shows angular symmetry with maximum radiated energy at a polar angle $\theta=0°$ and minimum at $\theta=90°$. As the intensity is increased to 2×10^{18} W/cm^2 the interaction becomes relativistic ($\gamma\approx1.5$), which destroys the polar angle dipole radiation pattern symmetry. Furthermore, a clear distinction can be made between a classically ionized electron and coherent radiation treatment from a tunneling probability current. Since the radiation is identical for both methods at $\theta=0°$ [Figs. 4(c)–4(f)] and is increasingly different as one looks in $\vec{x}$ away from k, one can infer the distinction between the two cases has an origin in interference since there is no phase difference in the propagation direction.

As the laser intensity is increased to 1.2×10^{19} W/cm^2 ($\gamma\approx4$) the radiation is peaked at $\theta=60°$ and resembles more closely the radiation pattern expected for relativistic accelerated charge. For a laser intensity of 5×10^{19} W/cm^2 ($\gamma\approx12$) the radiation yield from a classically ionized electron is singly peaked at a polar angle $\theta\approx30°$ while radiation from semiclassical ionization treatment with coherent averaging has two peaks located at $\theta\approx0°$ and $\theta\approx30°$. As mentioned, the radiation yield from the two treatments of ionization at a polar angle $\theta\approx0°$ is identical; however, as one sweeps to larger polar angles towards the secondary peak at $\theta\approx30°$ the radiation yield from coherently summed tunneling probability current is drowned by a factor of approximately 50 due to interference. In Fig. 4(f) at 1.2×10^{20} W/cm^2 the electron motion is ultrarelativistic with a peak $\gamma\approx30$, radiation emitted at $\theta\approx20°$ and an incredible factor of 100 difference in the peak radiation yield from coherent tunneling ionization probability current compared to that of a classically ionized electron.

C. Radiation from classical and semiclassical ionization in a pulsed focused laser field

Until now we have discussed only the results for a single ionization event in a 1D plane wave laser pulse. In this section we include radiation in a three-dimensional high intensity laser focus where multiple atoms and/or ions are distributed randomly and uniformly in the laser focus. The density of atoms is varied to converge on a density independent result while avoiding interatomic spacing effects [50].

Figure 5 shows the total radiated energy from classical MC ADK ionization and SC coherent ionization in a three-dimensional laser pulse. The radiation yield is normalized in the figure to the total amount of photoionization with units of energy per photoelectron (eV/electron). Figure 5 shows at intensities of 10^{17} W/cm^2 and less, highlighted as region I in the figure, there is slightly more of a difference between W_c and $W_{\text{SC-coherent}}$ compared to Fig. 6(a). Overall though, the results are consistent with the 1D plane wave results. Any difference from the plane wave case is expected to be rooted in the increased drift energy of the electron from the acceleration of the photoelectron out of the focus. For laser intensities in the range (2×10^{17} W/cm^2 to 5×10^{19} W/cm^2, Figs. 5 and 6), the results in the focal geometry case are qualitatively identical to those for the one-dimensional analysis, i.e., a reduction in the high-frequency radiation due to interference in the extended tunneling ionization probability current compared to the "perfect" coherence of a point classical electron.

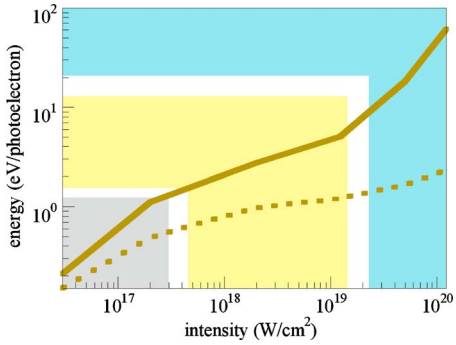

FIG. 5. (Color online) Radiated energy versus laser intensity from classical photoionization (solid), and coherently summed tunneling probability current (dotted). Three regions (see text) are highlighted in the figure.

Closer examination of Fig. 2 and Fig. 5, however, reveals a significant difference between the idealized 1D case and the 3D focal geometry used in experiments. In regions II and III, the quantitative yields do not agree. Beginning at about 10^{18} W/cm^2 the yields diverge. While in the one-dimensional case the radiated energy for the incoherent (coherent) mechanism increases as $I^{1.5}$ ($I^{0.8}$) in region II to $I^{1.8}$ ($I^{1.1}$) for region III, for the 3D case the intensity dependence in region II is only $I^{0.34}$ ($I^{0.11}$) and $I^{1.36}$ ($I^{0.4}$) in region III. By a few times 10^{19} W/cm^2, all radiation yields are 10 times lower for the focal geometry case than the respective yields in the plane wave case. This difference in the intensity dependence is due to electron-electron interferences between atoms ionized at different locations in a laser focus. Compar-

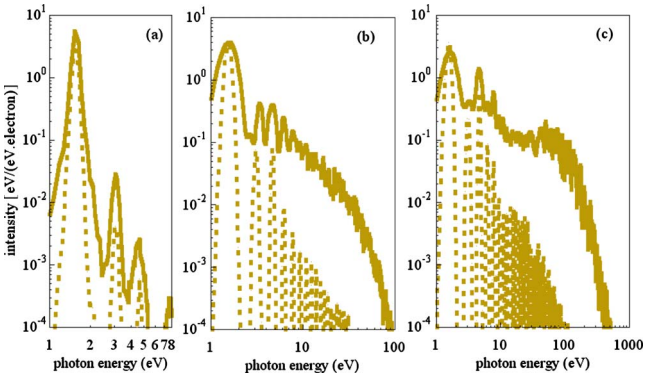

FIG. 6. (Color online) Total spectral amplitude of the radiated field from atomic ionization at intensities (a) 2×10^{17} W/cm^2, (b) 1.2×10^{19} W/cm^2, and (c) 5×10^{19} W/cm^2 from classical photoionization (solid) and coherently summed tunneling probability current (dotted).

ing the results at the peak intensity of 10^{20} W/cm^2 the coherent superposition of the radiation across the focal geometry has a larger effect than any difference in the way the ionization is treated; the degree of the coherence of the radiation across the focus can affect the radiation yield to a greater extent than the incoherent or coherent treatment of the radiation during the ionization process. Figure 6 is a plot of the power spectrum for the radiated harmonics at three different focal intensities. As one compares Fig. 3(c) to Fig. 6(c) the absolute difference in the radiation is 100 times for the first few harmonics and 1000 times for the radiation near 100 eV.

D. Angle and energy resolved radiation yield for ionization in a pulsed focused laser field

The angle and energy resolved radiation yields are presented in Fig. 7 for the focal geometry case. The plots are comparable to Fig. 3 but offer the additional derivative of the yields as a function of frequency. The radiation from classically ionized photoelectrons (essentially synonymous with the incoherently summed tunneling probability current) are shown in Figs. 7(a), 7(c), 7(e), 7(g), and 7(i) and the coherent tunneling probability current results in Figs. 7(b), 7(d), 7(f), 7(h), and 7(j). The logarithmic scale used in the plot is normalized to the peak radiation yield from classically ionized electrons in the respective laser field intensity.

An inspection of Fig. 7 reveals as one progresses beyond the dipole response [Figs. 7(a) and 7(b)] to ultrahigh fields coherently interfering radiation consistently occurs at larger angles in θ compared to incoherently summed or classical ionization. Furthermore, the cutoff, or high-frequency radiation, is always lower for coherently summed radiation by factors of 3 to 4 when the intensities are between 10^{19} W/cm^2 and 10^{20} W/cm^2. This poses some difficulty for experiments since the difference between coherent and incoherent radiation is similar to the difference one would expect by a simple change in intensity. The possibility for confusion in this case of alternate causality can be seen by comparing, for example, Fig. 7(h) for coherent radiation at 5×10^{19} W/cm^2 with Fig. 7(e) for incoherent radiation at 1.2×10^{19} W/cm^2. Similar comparisons can be made for Fig. 7(j) to Fig. 7(g). This observation combined with the N^2 effect of the focal geometry, the clearest identification of coherence from radiation in ultrastrong fields may come from the intensity dependence of the radiated power.

The radiation yield from the highest intensities studied involve photoionization at a peak intensity of 1.2×10^{20} W/cm^2. The radiation is peaked at a polar angle ($\theta\sim34°$) for classically ionized electrons and ($\theta\sim45°$) semiclassical ionization case with a cutoff photon energy for classically ionized electrons extending out to ($h\nu\sim1.75$ keV) while for semiclassical ionization it extends out to ($h\nu\sim420$ eV).

IV. CONCLUSION

These results on the radiation from ultrahigh-field ionized atoms have characterized the role of coherence on the yield from the dipole response up to the currently known limit of tunneling ionization at 10^{20} W/cm^2. We find a classical view

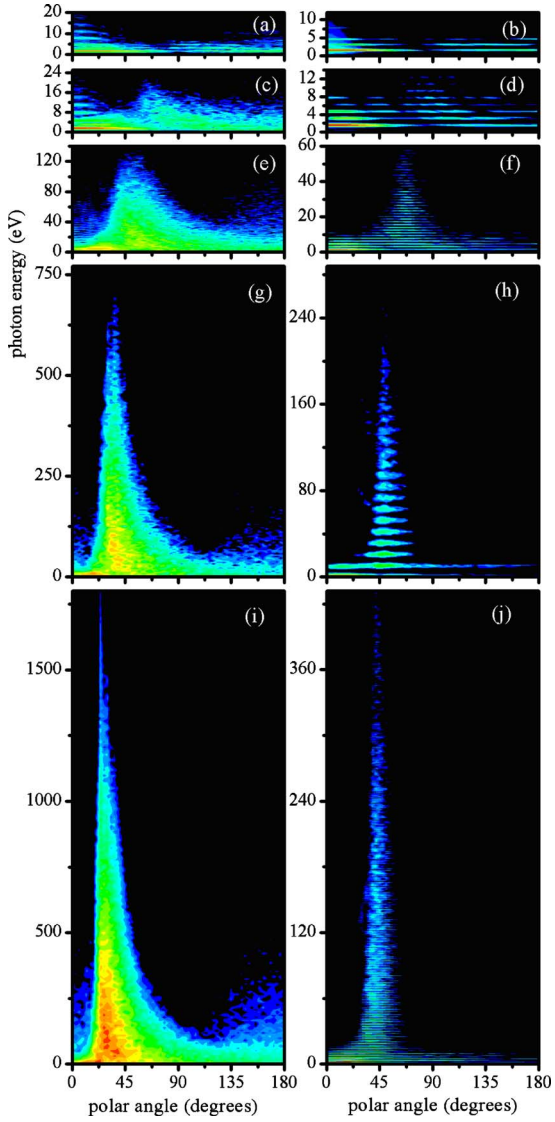

FIG. 7. (Color online) Angle- and frequency-resolved total radiation yield for (a),(b) 2×10^{17} W/cm^2, (c),(d) 2×10^{18} W/cm^2, (e),(f) 1.2×10^{19} W/cm^2, (g),(h) 5×10^{19} W/cm^2, and (i),(j) 1.2×10^{20} W/cm^2 for classical (a), (c), (e), (g), (i) and coherently summed tunneling probability current (b), (d), (f), (h), (j).

of ionization results in the same yield as a tunneling ionization probability current treatment when the radiation sum across the current is done incoherently. In the case that one assumes perfect coherence of the radiation across the tunneling current, the observed radiation decreases when the excursion of the photoelectron is comparable to the wavelength of the emitted radiation due to interference in the far field. When comparing the plane wave case to the focal geometry, the coherence of the radiation across the micrometer spatial extend of the focus has a larger affect on the observed yields the degree of coherence within the tunneling ionization current and interference from the photoelectron excursion α_0 for a single photoionization event. Additional difficulties may be faced by experimental studies because changes in the coherence and changes in the intensity can have a similar effect on the observed radiation.

[1] M. D. Perry and G. Mourou, Science **264**, 917 (1994).
[2] D. M. Pennington, C. G. Brown, T. E. Cowan, S. P. Hatchett, E. Henry, S. Herman, M. Kartz, M. Key, J. Koch, A. J. MacKinnon, M. D. Perry, T. W. Phillips, M. Roth, T. C. Sangster, M. Singh, R. A. Snavely, M. Stoyer, B. C. Stuart, and S. C. Wilks, IEEE J. Sel. Top. Quantum Electron. **6**, 676 (2000).
[3] C. N. Danson, P. A. Brummitt, R. J. Clarke, I. Collier, B. Fell, A. J. Frackiewicz, S. Hawkes, C. Hernandez-Gomez, P. Holligan, M. H. R. Hutchinson, A. Kidd, W. J. Lester, I. O. Musgrave, D. Neely, D. R. Neville, P. A. Norreys, D. A. Pepler, C. Reason, W. Shaikh, T. B. Winstone, R. W. W. Wyatt, and B. E. Wyborn, Laser Part. Beams **23**, 87 (2005).
[4] B. Walker, C. Toth, D. Fittinghoff, T. Guo, D. Kim, C. Rose-Petruck, J. Squier, K. Yamakawa, K. Wilson, and C. Barty, Opt. Express **5**, 196 (1999).
[5] A. DiChiara, E. A. Chowdhury, G. Ongadi, B. C. Walker, and R. S. Tamosaitis, Opt. Lett. **28**, 2106 (2003).
[6] S. Witte, R. Th. Zinkstok, A. L. Wolf, W. Hogervorst, W. Ubachs, and K. S. E. Eikema, Opt. Express **14**, 8168 (2006).
[7] E. L. Clark, K. Krushelnick, M. Zepf, F. N. Beg, M. Tatarakis, A. Machacek, M. I. K. Santala, I. Watts, P. A. Norreys, and A. E. Dangor, Phys. Rev. Lett. **85**, 1654 (2000).
[8] T. E. Cowan, A. W. Hunt, T. W. Phillips, S. C. Wilks, M. D. Perry, C. Brown, W. Fountain, S. Hatchett, J. Johnson, M. H. Key, T. Parnell, D. M. Pennington, R. A. Snavely, and Y. Takahashi, Phys. Rev. Lett. **84**, 903 (2000).
[9] A. Heidenreich, I. Last, and J. Jortner, J. Chem. Phys. **127**, 074305 (2007).
[10] D. Umstadter, J. Phys. D **36**, R151 (2003).
[11] J. Z. Wu, J. H. Cooley, T. V. Antonsen, and H. M. Milchberg, Phys. Plasmas **12**, 043105 (2005).
[12] T. Ditmire, S. Bless, G. Dyer, A. Edens, W. Grigsby, G. Hays, K. Madison, A. Maltsev, J. Colvin, M. J. Edwards, R. W. Lee, P. Patel, D. Price, B. A. Remington, R. Sheppherd, A. Wooton, J. Zweiback, E. Liang, and K. A. Kielty, Radiat. Phys. Chem. **70**, 535 (2004).
[13] F. He, Y. Y. Lau, D. P. Umstadter, and T. Strickler, Phys. Plasmas **9**, 4325 (2002).
[14] S. Y. Chen, A. Maksimchuk, and D. Umstadter, Nature (London) **396**, 653 (1998).
[15] C. I. Moore, J. P. Knauer, and D. D. Meyerhofer, Phys. Rev. Lett. **74**, 2439 (1995).
[16] A. Ting, D. Kaganovich, D. F. Gordon, R. F. Hubbard, and P. Sprangle, Phys. Plasmas **4**, 1889 (1997).
[17] D. D. Meyerhofer, J. P. Knauer, S. J. McNaught, and C. I. Moore, J. Opt. Soc. Am. B **13**, 113 (1996).
[18] E. A. Chowdhury, I. Ghebregziabher, J. MacDonald, and B. C. Walker, Opt. Express **12**, 3911 (2004).
[19] I. Ghebregziabiher, S. Palaniyappan, J. MacDonald, and B. C. Walker, Phys. Rev. A **73**, 033419 (2006).
[20] S. Palaniyappan, I. Ghebregziabher, A. DiChiara, J. MacDonald, and B. C. Walker, Phys. Rev. A **74**, 033403 (2006).
[21] Youwei Tian, Wei Yu, Feng He, Han Xu, Vinod Senecha, Degang Deng, Yi Wang, Ruxin Li, and Zhizhan Xu, Phys. Plasmas **13**, 123106 (2006).
[22] E. A. Chowdhury, I. Ghebregziabiher, and B. C. Walker, J. Phys. B **38**, 517 (2005).
[23] J. Faure, Y. Glinec, A. Pukhov, S. Kiselev, S. Gordienko, E. Lefebvre, J. P. Rousseau, F. Burgy, and V. Malka, Nature (London) **431**, 541 (2004).
[24] F. Sohbatzadeh, S. Mirzanejhad, and M. Ghasemi, Phys. Plasmas **13**, 123108 (2006).
[25] Xinkui He, B. Shuai, X. C. Ge, R. X. Li, and Z. Z. Xu, Phys. Rev. E **68**, 056501 (2003).
[26] Y. I. Salamin and C. H. Keitel, Phys. Rev. Lett. **88**, 095005 (2002).
[27] G. R. Mocken and C. H. Keitel, Comput. Phys. Commun. **166**, 171 (2005).
[28] K. TaPhuoc, A. Rousse, M. Pittman, J. P. Rousseau, V. Malka, S. Fritzler, D. Umstadter, and D. Hulin, Phys. Rev. Lett. **91**, 195001 (2003).
[29] S. Palaniyappan, A. DiChiara, E. A. Chowdhury, A. Falkowski, G. Ongadi, E. L. Huskins, and B. C. Walker, Phys. Rev. Lett. **94**, 243003 (2005).
[30] P. B. Corkum, Phys. Rev. Lett. **71**, 1994 (1993).
[31] Y. Ueshima, Y. Kishimoto, A. Sasaki, and T. Tajima, Laser Part. Beams **17**, 1 (1999).
[32] J. Tate, T. Auguste, H. G. Muller, P. Salieres, P. Agostini, and L. F. DiMauro, Phys. Rev. Lett. **98**, 013901 (2007).
[33] P. Tomassini, M. Galimberti, A. Giulietti, D. Giulietti, L. A. Gizzi, and L. Labate, Phys. Plasmas **10**, 917 (2003).
[34] K. Lee and Y. H. Cha, Opt. Express **11**, 309 (2003).
[35] S. K. Ride, E. Esarey, and M. Baine, Phys. Rev. E **52**, 5425 (1995).
[36] C. H. Keitel and P. L. Knight, Phys. Rev. A **51**, 1420 (1995).
[37] Yousef I. Salamin, J. Phys. A **30**, 4399 (1996).
[38] G. A. Krafft, A. Doyuran, and J. B. Rosenzweig, Phys. Rev. E **72**, 056502 (2005).
[39] S. X. Hu and A. F. Starace, Phys. Rev. Lett. **88**, 245003 (2002).
[40] P. Krekora, R. E. Wagner, Q. Su, and R. Grobe, Laser Phys. **12**, 455 (2002).
[41] T. Tritschler, K. D. Hof, M. W. Klein, and M. Wegener, Opt. Lett. **30**, 753 (2005).
[42] S. Palaniyappan, A. DiChiara, I. Ghebregziabher, E. L. Huskins, A. Falkowski, D. Pajerowski, and B. C. Walker, J. Phys. B **39**, S357 (2006).
[43] J. P. Barton and D. R. Alexander, J. Appl. Phys. **66**, 2800 (1989).
[44] L. W. Davis, Phys. Rev. A **19**, 1177 (1979).
[45] I. Ghebregziabher and B. C. Walker, Phys. Rev. A **76**, 023415 (2007).
[46] M. V. Ammosov, N. B. Delone, and V. P. Krainov, Sov. Phys. JETP **64**, 1191 (1986).
[47] A. M. Perelomov, V. S. Popov, and M. V. Terent'ev, Zh. Eksp. Teor. Fiz. **50**, 1393 (1966) [Sov. Phys. JETP **23**, 924 (1966)].
[48] V. S. Popov, Phys. Usp. **47**, 855 (2004).
[49] J. D. Jackson, *Classical Electrodynamics* 2nd ed. (Wiley, New York, 1975), p. 654.
[50] A. Bandrauk (unpublished).